THE JOURNAL OF PHYSICAL CHEMISTRY C

ARTICLE

pubs.acs.org/JPCC

# Understanding the Promotion Effect of Lanthanum Oxide on Gold-Based Catalysts in the Partial Oxidation of Methanol by in Situ XAFS and DSC Studies

Bart P. C. Hereijgers,[†] Tamara M. Eggenhuisen,[†] Krijn P. de Jong,[†] Herre Talsma,[‡] Ad M. J. van der Eerden,[†] Andrew M. Beale,[†] and Bert M. Weckhuysen*[,†]

[†]Inorganic Chemistry and Catalysis Group, Debye Institute for NanoMaterials Science, and [‡]Department of Pharmaceutics, Utrecht Institute for Pharmaceutical Sciences, Utrecht University, Universiteitsweg 99, 3584 CG, Utrecht, The Netherlands

**ABSTRACT:** Promoting supported gold nanoparticles with lanthanum oxide largely increases the hydrogen selectivity in the partial oxidation of methanol. In this study, the origin of the promotion effect of lanthanum oxide on supported gold catalysts was investigated. The formation of small gold nanoparticles on both the high surface area alumina and the low surface area lanthanum oxide support materials was confirmed by Transmission Electron Microscopy (TEM) and Extended X-ray Absorption Fine Structure (EXAFS). In situ X-ray absorption spectroscopy during partial methanol oxidation revealed the formation of oxidized gold species on the reduced $Au/Al_2O_3$ catalyst material, whereas $La_2O_3$ was found to facilitate the reduction of initially present oxidic gold species. This was confirmed by a larger measured heat of reaction for the exothermic decomposition of the oxidic gold species supported on lanthanum oxide as was found by differential scanning calorimetry. The catalysts under study did not show significant differences in methanol oxidation activity; however, the $Au/Al_2O_3$ catalyst exhibited much higher activity in CO and $H_2$ oxidation. These observed differences in catalytic activity and selectivity of the $Al_2O_3$- and $La_2O_3$-supported Au catalysts are explained by the differences in redox behavior of the gold nanoparticles. It is proposed that zerovalent gold species limit dissociative $H_2$ adsorption during the partial oxidation of methanol and thus improve the $H_2$ selectivity by reducing $CH_4$ and $H_2O$ formation.

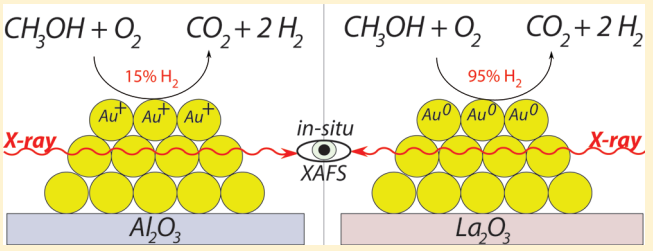


## INTRODUCTION

Since the discovery that supported gold nanoparticles supported on oxidic support materials display remarkable catalytic activity in hydrogenation,[1] oxidation,[2] and hydrochlorination[3] reactions, many studies have been conducted on the properties of this precious metal as a heterogeneous catalyst.[4−9] Although gold catalysts have been applied in many catalytic processes, the vast majority of publications describes the use of supported gold-based catalysts in selective oxidation reactions, among which the low-temperature oxidation of CO received the most attention by far.

One reaction that has been studied less extensively is the partial oxidation of methanol (POM) for the production of $H_2$ from methanol for fuel cell electrochemical combustion.[10−16] In essence, $H_2$ for automotive applications can be supplied in two different manners. The first is based on hydrogen storage technologies, i.e., in high-pressure tanks, by cryogenic methods, or bonded in an inorganic matrix, which all have their advantages and challenges.[17] An alternative for storage is the on-board generation of $H_2$ from light, sustainably produced hydrocarbons.[18] For the latter option, methanol (MeOH) is a preferred source due to its wide availability and consequent low price, the high $H_2$ content of 12 wt %, and the ease of applicability in the present liquid petrol infrastructure. In addition to mobile applications, such a hydrogen "storage" method can be of interest for small, on-site, hydrogen-consuming devices, especially at remote locations as well.

Besides POM, there are other routes for $H_2$ generation from MeOH reported in the literature, e.g., methanol decomposition,[19] steam reforming,[20] and autothermal reforming.[21−23] The obvious advantage POM offers over reforming processes is that it uses air as oxidant instead of high energy demanding steam. In addition, POM is an exothermic reaction, so no heat supply to the reaction is needed. The major challenge in POM is to reduce CO formation to a minimum (<10 ppm) to make the $H_2$ applicable in a low-temperature proton exchange membrane fuel cell.[18] However, recent advances in fuel cell membrane technologies led to the development of membranes capable of operating at higher temperature, increasing the fuel cell Pt anode resistance to higher CO concentrations.[24,25] Supported gold catalysts have shown the ability to produce $H_2$ from MeOH with significantly lower CO content as compared to, e.g., Cu/ZnO-based catalyst systems.[10−15]

Recently we described that the selectivity of $\gamma$-$Al_2O_3$-supported gold catalysts in POM for $H_2$ production with very low

**Received:** May 26, 2011
**Revised:** July 6, 2011
**Published:** July 07, 2011

CO content can be largely improved by the addition of alkaline earth metal and lanthanum oxides.[16] In the current contribution, the promotion effect of lanthanum oxide on the catalytic performance in MeOH, CO, and $H_2$ oxidation is studied by in situ X-ray Absorption Spectroscopy (XAS), theoretical simulations of XAS spectra, and Differential Scanning Calorimetry (DSC) together with catalytic activity tests. To the best of our knowledge, this is the first in situ study into the active catalytic site for POM on gold-based catalysts.

## EXPERIMENTAL PROCEDURES

**Catalyst Preparation.** Catalyst materials were prepared as described elsewere.[16] Promoted catalyst materials were prepared by Incipient Wetness Impregnation of aqueous $Ba(NO_3)_2$ (Fluka, 99%) and $La(NO_3)_3$ (Alfa Aesar, 99%) solutions containing the amount of Ba and La to obtain a Au/M molar ratio of 5 on 2 g of $\gamma$-$Al_2O_3$ (Engelhard, $S_{BET}$ = 230 $m^2\ g^{-1}$, pore volume = 0.76 mL $g^{-1}$). For the Au/$La_2O_3$ catalyst, lanthanum oxide (Merck 99.9%, $S_{BET} \sim 1\ m^2\ g^{-1}$) was used.

After impregnation of $Ba(NO_3)_2$ or $La(NO_3)_3$, the catalysts were dried at 60 °C overnight and calcined in stagnant air at 700 °C for 6 h. Gold deposition was done following a deposition precipitation procedure. The (promoted) support was dispersed in 50 mL of deionized water, and the pH was adjusted to 9.5 with diluted aqueous $NH_4OH$ (Merck, 25%). An amount of $HAuCl_4$ in dilute HCl (Sigma Aldrich, 99.99% trace metal basis) to obtain a weight loading of 1 wt % was dissolved in 30 mL of water and slowly added to the support slurry while maintaining a constant pH of 9.5 by addition of $NH_4OH$ (aq). After addition, the slurry was stirred for another 30 min and filtered, washed thoroughly with demi-water to remove all chloride, and dried at 60 °C. The samples were calcined at 200 °C in stagnant air for 4 h. For the samples for DSC analysis, an amount of $HAuCl_4$ solution to obtain a Au weight loading of 2.5 wt % was used for deposition precipitation. The samples were dried under $N_2$ flow at room temperature and not subjected to any heat treatment.

**Catalyst Characterization.** Diffuse Reflectance UV−vis−NIR (DR) spectra were recorded on a Varian Cary 500 Spectrometer using a white Halon standard for background subtraction. Inductively Coupled Plasma Atomic Emission Spectroscopy (ICP-AES) analysis of the gold loading of the uncalcined catalyst samples was performed by Mikroanalytische Laboratorium KOLBE (Mülheim an der Ruhr, Germany). Prior to analysis, the samples were dried at 20 °C under vacuum.

The decomposition behavior of the gold catalysts was studied by DSC (TA Instruments Q2000). The temperature and heat flow were calibrated using a certified indium sample.[26] Prior to analysis, 9−20 mg of sample was dried under dynamic vacuum overnight to remove physisorbed water. The aluminum sample pans (TA Instruments Tzero hermetic pans/lids) were subsequently brought into the $N_2$ atmosphere and hermetically closed to prevent readsorption of atmospheric water. Just before analysis, the lid of the sample pan was pierced several times to allow the evaporation of water evolving from the sample. DSC was measured from 0 to 250 °C with a scanning rate of 2 °C $min^{-1}$ in a $N_2$ flow of 50 mL $min^{-1}$. Thermogravimetric Analysis (TGA, TA Instruments Q50) was done from room temperature to 250 °C with the same rate in a $N_2$ flow of 60 mL $min^{-1}$.

Extended X-ray Absorption Fine Structure (EXAFS) characterization of the Au $L_{III}$ edge was performed at the European Synchrotron Radiation Facility (ESRF, Grenoble France) at beamline BM 26A.[27] The ESRF synchrotron operated at 6 GeV with a typical current between 150 and 250 mA. The station was equipped with a Si(111) double-crystal monochromator and two vertically focusing Pt- and Si-coated mirrors for harmonic rejection. X-ray absorption spectra were recorded in fluorescence mode using a nine-element monolithic germanium fluorescence detector. In situ X-ray Absorption Near Edge Structure (XANES) spectra were recorded at the Hasylab facility in Hamburg (Germany) at beamline X1. The Hasylab synchrotron operated at 4.44 GeV, and the ring current was between 140 and 80 mA. The monochromator double Si(111) crystals were detuned to 70% of the intensity to eliminate higher harmonics. Spectra were measured in fluorescence mode using a five-element germanium detector.

Typically, ∼100 mg of sample was gently pressed into a self-supporting wafer and placed in a stainless steel in situ cell designed for XAFS measurements. EXAFS spectra were recorded at 120 °C in He flow. In situ XANES spectra were recorded under POM conditions (10 vol % MeOH and 5 vol % $O_2$ in He) at 300 °C. An aluminum foil was used between the sample and the detector to reduce La and Ba $L_\alpha$ and $L_\beta$ fluorescence radiation. By placing an Au foil between a second and third ion-chamber detector, any drift in the energy calibration of the beamline can be eliminated.

XAFS data were evaluated using the IFEFFIT software package programs Athena (raw data conversion, normalization, and background subtraction to extract the EXAFS from the spectra) and Artemis (to perform a least-squares fitting of the experimental data).[28,29] An amplitude reduction factor ($S_0^2$) of 0.85 was obtained from fitting the experimental spectrum of a gold foil with fixed coordination numbers and used to extract coordination numbers for the gold nanoparticles. The experimental spectra were fitted in *R*-space, and multiple scattering contributions were considered but found to pay a negligible contribution in the first shell fit and thus ignored.

Theoretical spectra on the Au $L_{III}$ edge were obtained from self-consistent full multiple scattering simulations using the FEFF8 code. A Hedin−Lundqvist potential and the $L_{III}$ XANES, LDOS, NOHOLE (for complete core-hole screening), Self-Consistent Field (SCF), and Full Multiple Scattering (FMS) cards were used. The cluster used for the simulations was a spherical gold cluster of 1 nm diameter with FCC geometry ($r$ = 5.0 Å) and bulk bond distances ($R_{Au-Au}$ = 2.88 Å) and chosen to roughly match the gold particle size of the catalyst materials. The cluster contained 43 gold atoms ($Au_{43}$) arranged as one central atom with three full coordination shells. Atomic coordinates for the cluster were derived from crystallographic data using the ATOMS program. The atomic coordinates for the adsorbates were optimized using Forcite calculations in the Materials Studio (Accelrys) software. The positions of the gold atoms were constrained to the FCC lattice during structure optimization. Theoretical XANES spectra were simulated for the central atom, all coordination shells, and the atom bonding to the adsorbate as principle absorber and number weighted averaged.

**Catalytic Performance.** Catalytic test reactions were done in a quartz reactor with 100 mg of catalyst (212−425 $\mu$m sieve fraction). Prior to introducing reactive gases, the system was flushed with He. The gas flow consisted of 10% MeOH, obtained by flowing He through a MeOH saturator at 20 °C and 5% $O_2$ diluted to 50 mL $min^{-1}$ with $N_2$ (internal standard for GC). The composition of the product flow was analyzed with an online double channel CompactGC by Interscience equipped with a

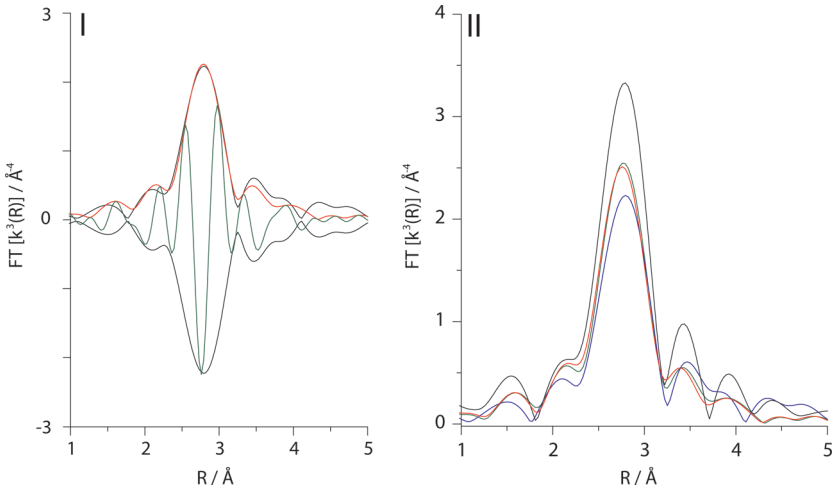


**Figure 1.** (I) Phase-corrected $k^3$-weighted Fourier-transformed EXAFS spectra and the least-squares first shell fits of fresh $Au/Al_2O_3$ catalyst material. Experimental FT spectrum (black) and fit: imaginary part (green) and magnitude (red). (II) Magnitudes of the phase corrected $k^3$-weighted FT-EXAFS spectra of $Au/Al_2O_3$ (blue), $AuBaO/Al_2O_3$ (red), $AuLa_2O_3/Al_2O_3$ (green), and $Au/La_2O_3$ (black).

**Table 1. EXAFS Fit Parameters and Corresponding Particle Diameter of Different Alumina and Lanthana Supported Gold Catalyst Materials after Calcination Compared With a Au Foil ($k^3$; $\Delta k$ = 2.4−9.5 Å$^{-1}$, $\Delta r$ = 1.7−3.5 Å)[a]**

| | | | | | particle size estimate (Å) | |
|---|---|---|---|---|---|---|
| catalyst | $R_{Au-Au}$ (Å) | $N_1$ (±10%) | Debye−Waller ($\sigma^2$) | $E_0$ (eV) | EXAFS | TEM |
| Au foil | 2.87 | 12 | 0.0079 | 2.75 | - | - |
| $Au/Al_2O_3$ | | | | | | |
| fresh | 2.78 | 5.9 | 0.013 | 1.28 | 8 | 35 |
| spent | 2.80 | 8.1 | 0.012 | 2.82 | 13 | |
| $AuBaO/Al_2O_3$ | | | | | | |
| Fresh | 2.75 | 5.0 | 0.010 | 1.6 | 7 | 29 |
| spent[b] | 2.77 | 6.1 | 0.012 | 2.53 | 11 | |
| $AuLa_2O_3/Al_2O_3$ | | | | | | |
| fresh | 2.76 | 6.0 | 0.012 | 1.75 | 8 | 19 |
| spent | 2.76 | 5.8 | 0.011 | 2.04 | 7 | |
| $Au/La_2O_3$ | | | | | | |
| fresh | 2.78 | 6.2 | 0.0097 | 1.8 | 9 | 31 |
| fresh[c] | 2.80 | 8.1 | 0.011 | 0.742 | 12 | 20 |
| spent[c] | 2.78 | 7.8 | 0.010 | 0.11 | 11 | - |

[a] EXAFS spectra were recorded at 120 °C in He flow. [b] The data were suffering from strong Ba $L_\alpha$ and $L_\beta$ fluorescence, resulting in noisy data and a relative large error for this measurement. Due to correlation problems, the Debye−Waller factor was constrained during fitting. [c] Data obtained at the Hasylab synchrotron.

PorabondQ and 5MS molsieve column and TC detectors. For the CO and $H_2$ oxidation experiments, a 50 mL min$^{-1}$ gas flow containing 3 mL min$^{-1}$ CO or $H_2$ and 3 mL min$^{-1}$ $O_2$ in He was used. All activity measurements were performed in a temperature-programmed reaction from room temperature to 300 °C with a heating rate of 2 °C min$^{-1}$, followed by an isothermal period.

## RESULTS

**Catalyst Characterization.** The catalyst materials have been characterized by UV−vis−NIR DR spectroscopy, EXAFS, and TEM. All gold-based catalysts exhibited a pink to purple color after calcination, caused by an absorption band at 500−550 nm due to the Au surface plasmon resonance, which is direct evidence for the formation of nanostructured metallic gold particles.[30] The fitted FT-EXAFS spectrum of $Au/Al_2O_3$ is presented in Figure 1(I). The theoretical fits described the experimental FT-EXAFS spectra of all catalyst materials under study in both the magnitude and the imaginary part (not shown) accurately. The fitting results, including the average particle sizes extracted from the EXAFS and TEM analysis, are presented in Table 1.[31−33] The average particle sizes were similar for all catalyst materials, although the $Au/La_2O_3$ catalyst material showed slightly larger particles. This is clearly observed from the increased amplitude of the Au−Au scattering at $R$ = 2.8 Å in


dx.doi.org/10.1021/jp204919z |J. Phys. Chem. C 2011, 115, 15545–15554

the FT-EXAFS spectra in Figure 1(II). The amplitude of the EXAFS is directly related to the Au coordination number.

The average particle diameter as obtained from TEM was larger than the value estimated from EXAFS. Moreover, the TEM analysis gave some variation in particle size between the different materials, though the average particle sizes derived from EXAFS are similar. This is most likely the effect of the contribution of subnanometer gold particles which remain invisible in TEM and illustrates the importance of EXAFS analysis. The mismatch between EXAFS and TEM particle size estimations for supported gold nanoparticles has been reported before.[34] It was observed that for the $Au/Al_2O_3$ and $AuBaO/Al_2O_3$ catalyst materials the Au particles seemed to grow a little during reaction at 300 °C. In the case of the lanthanum oxide containing samples, the particle diameter seemed stable over the reaction period or decreased slightly.

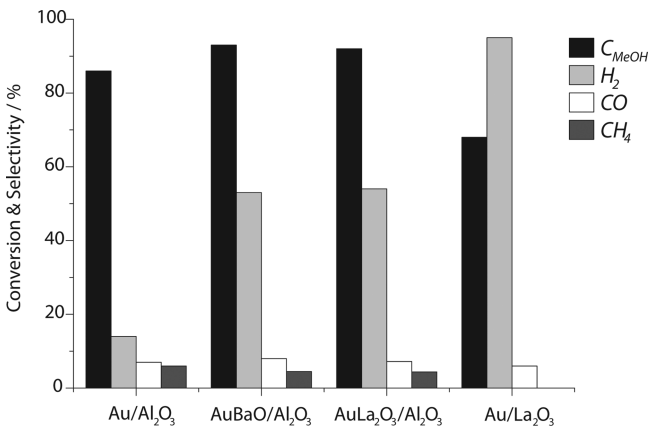


**Figure 2.** Methanol conversion and selectivity toward $H_2$, CO, and $CH_4$ in POM at 300 °C over the different gold-based catalyst materials.

The catalytic performance of the materials under study is summarized in Figure 2. As reported earlier,[16] when adding BaO or $La_2O_3$ to the $Au/Al_2O_3$ catalyst, the hydrogen selectivity increased from 15% to 55%. The $Au/La_2O_3$ exhibited superior performance in terms of $H_2$ selectivity (95%), although the conversion was lower. Over the $Au/La_2O_3$ catalyst material, only trace amounts ($\ll$1%) of methane formation were observed. Over plain lanthanum oxide, a methanol conversion of only 13% and no significant $H_2$ formation was observed at 300 °C, confirming that the supported gold nanoparticles are essential for activity and selectivity in this reaction.

**In Situ $\Delta\mu$-XANES Analysis during POM.** By performing a delta-mu ($\Delta\mu$) analysis of the in situ XANES spectra, small changes can be made more pronounced. $\Delta\mu$ analysis is usually performed by subtracting the spectrum of the material in an inert atmosphere from a spectrum of the same material, measured in the same experimental run at the same beamline, but under different reaction conditions.[35,36] In our case, the reference spectrum was recorded at 300 °C in a He flow and was subtracted from the in situ XANES spectra and recorded at 300 °C in a flowing mixture of MeOH and $O_2$ in He (POM conditions). $\Delta\mu$-XANES analysis has been successfully applied in the past to reveal bonding of species on noble metal catalyst systems, especially for Pt- and Au-based catalysts, and has become an established analysis method.[37−52]

Figure 3 displays the in situ XANES spectra recorded on the Au $L_{III}$ edge at 300 °C in He and during partial oxidation of methanol. In the normalized XANES spectra, no significant changes can be observed, which indicates that there are neither large changes in the oxidation state of the reactive gold particles

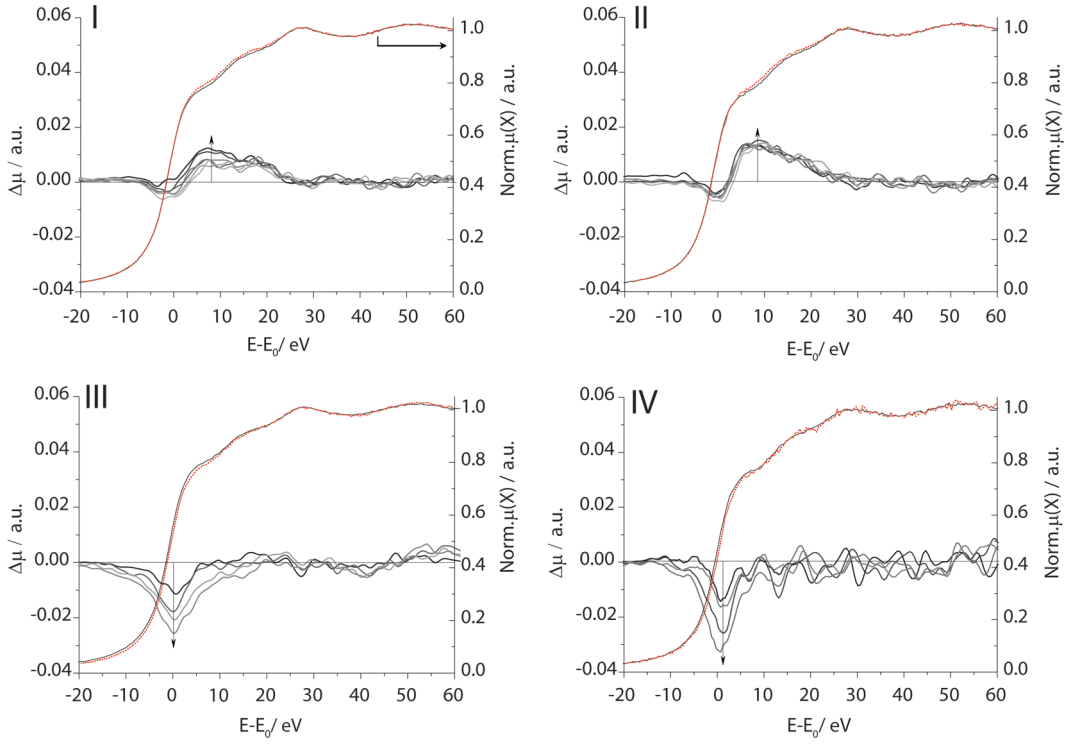


**Figure 3.** In situ XANES and $\Delta\mu$-XANES spectra of $Au/Al_2O_3$ (I), $AuBaO/Al_2O_3$ (II), $AuLa_2O_3/Al_2O_3$ (III), and $Au/La_2O_3$ (IV) during POM at 300 °C. Spectrum in He (black line), spectrum in reaction atmosphere (red line), and the difference spectra (gray line). The $\Delta\mu$-XANES spectra were smoothed by an iterative interpolating algorithm for clarity.


dx.doi.org/10.1021/jp204919z |J. Phys. Chem. C 2011, 115, 15545–15554

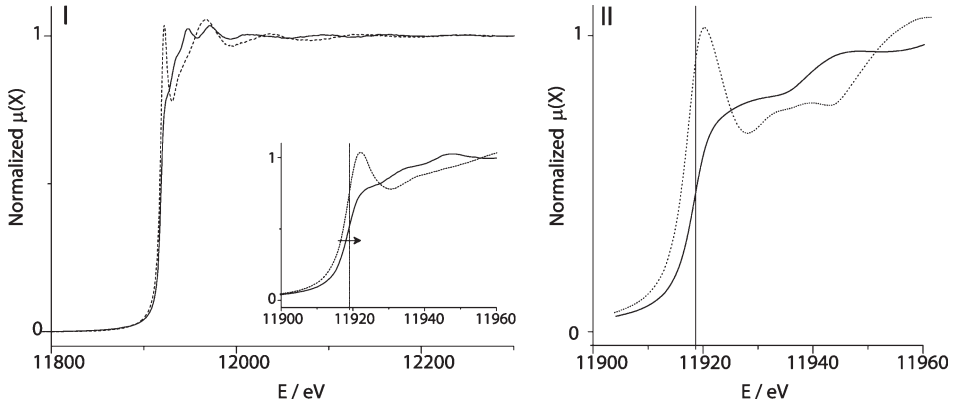


**Figure 4.** (I) Normalized experimental EXAFS spectra of the Au $L_{III}$ edge of $Au/Al_2O_3$ (solid line) and the uncalcined $Au(OH)_x/Al_2O_3$ catalyst (dashed line) and magnification of the XANES region (insert) showing the edge energy shift upon reduction and (II) simulated XANES spectra of a 1 nm metallic gold cluster (solid line) and a $Au_2O_3$ cluster (dashed line). The theoretical $Au^0$ $L_{III}$ edge energy at 11 919 eV is indicated.

during reaction nor significant modification of the gold particles size. The EXAFS results on the spent catalysts did not reveal excessive particle growth either.

It was observed that in the cases of $Au/Al_2O_3$ and $AuBaO/Al_2O_3$ (Figure 3I and II) catalysts a slight dip appeared at the edge position ($E_0$) in the $\Delta\mu$ signatures, with the simultaneous development of a positive feature at 5−20 eV over the edge. In the literature, comparable phenomena were observed for instance upon exposing gold nanoparticles to propene,[38] ethene,[40] and hydrogen[42] and during CO oxidation.[43,44] The appearance of a positive feature at or just over the edge position is caused by depletion of the Au d-band or, in other words, the formation of cationic surface gold atoms ($Au^{\delta+}$).[53] In a comprehensive study into the chemisorption of hydrogen on $Au/Al_2O_3$ and $Pt/Al_2O_3$ by Bus et al.,[41,42] $\Delta\mu$-XANES spectra were measured on the Au $L_{II}$ and $L_{III}$ edges, which show strong similarity with the $\Delta\mu$-XANES spectra under POM conditions on $Au/Al_2O_3$ and $AuBaO/Al_2O_3$. Bus et al. observed isotopic scrambling by cofeeding $H_2$ and $D_2$ over the catalyst and were able to assign the features in the $\Delta\mu$-XANES spectra to dissociative hydrogen chemisorption on Au and Pt clusters. On the basis of these reported findings and the results reported here, we propose that dissociative hydrogen chemisorption takes place on $Au/Al_2O_3$ and $AuBaO/Al_2O_3$ under POM conditions as well. Dissociative adsorption of $H_2$ on the gold catalyst is in line with the observed methane formation over alumina (promoted) supported gold catalysts,[16] originating either from methanation of CO or $CO_2$[54] or from the reaction of adsorbed atomic hydrogen with methanol.[10,55]

On the lanthanum promoted and supported catalyst materials, different features in the $\Delta\mu$-XANES spectra are observed. In Figure 3 (III and IV) it is clearly visible that under POM conditions a negative feature appears at the edge position. Also, such a negative feature has been reported before. Nijhuis et al. described the appearance of a negative peak at the edge position during activation of a $Au/SiO_2$ catalyst for $H_2$ oxidation, which they ascribed to the reduction of initially present cationic gold species.[38] The negative peak is caused by a small shift in the edge to higher energy upon reduction as illustrated in Figure 4 and was reported as well by Costello et al.[56] For the lanthanum oxide promoted and supported catalysts, no cationic gold species formation or hydrogen chemisorption was observed in the $\Delta\mu$-XANES spectra. It seems that under POM conditions these

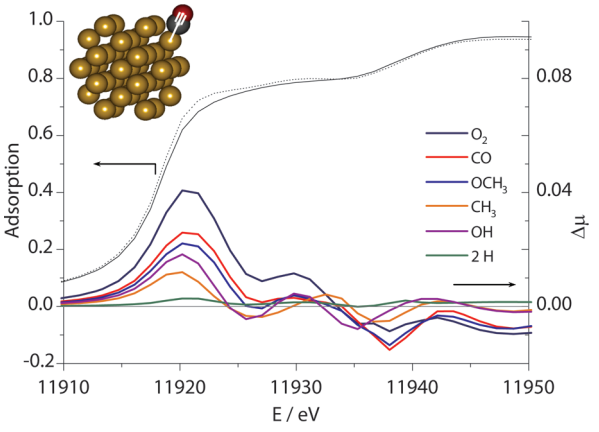


**Figure 5.** XANES spectra simulated using the FEFF8 code of a $Au_{43}$ cluster ($r$ = 5 Å) (solid line) and the depicted $Au_{43}CO$ cluster (dashed line) and $\Delta\mu$-XANES signatures of $Au_{43}$ clusters with different possible reaction intermediates adsorbed atop on the gold cluster.

catalyst materials reduce further, and lanthanum oxide is preventing the Au clusters from reoxidizing. This is confirmed by the fact that even an uncalcined $Au/La_2O_3$ catalyst material reduced rapidly during a temperature-programmed POM reaction, while the catalytic performance was not significantly altered. The reduction was confirmed by the color change from light yellow to pink, indicative of the formation of metallic nanosized gold particles.[30]

**FEFF8 Simulations.** Theoretical calculations on the Au $L_{III}$ edge using the FEFF8 code were performed to simulate $\Delta\mu$-XANES signatures caused by different species adsorbed atop on a $Au_{43}$ cluster. The FEFF8 code is highly suitable for good reproduction of XAS spectra of small metal clusters[57] and has been applied successfully before to get a theoretical fundament for experimental XANES spectra interpretation and gave insight into, e.g., the adsorption modes of ethene and CO to gold clusters.[40,43,44,58]

The simulated spectra of the Au $L_{III}$ near edge region of $Au_{43}$ and $Au_{43}CO$ are shown in Figure 5, together with the $\Delta\mu$-XANES signatures obtained from simulated spectra on $Au_{43}$ clusters with different adsorbates. The Au−C and C−O bond in $Au_{43}CO$ measured 1.967 and 1.128 Å, respectively, which are realistic values. The simulated spectra of both Au and $Au_2O_3$


dx.doi.org/10.1021/jp204919z |J. Phys. Chem. C 2011, 115, 15545–15554

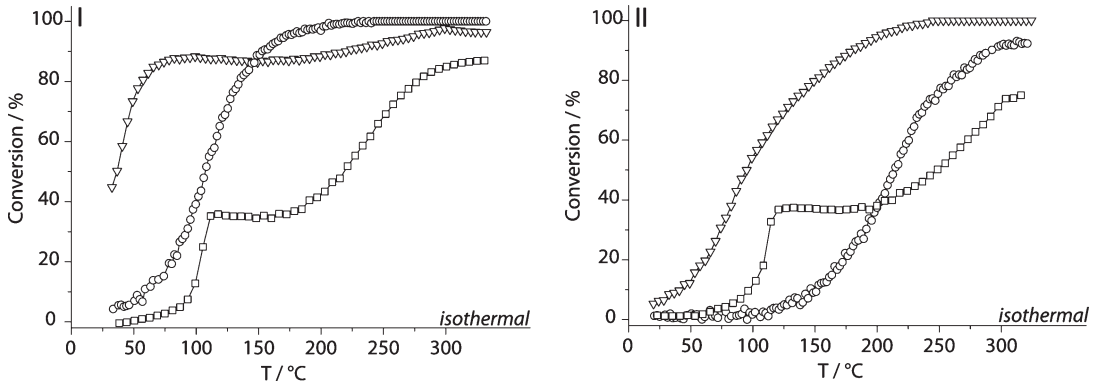


**Figure 6.** Catalytic performance of $Au/Al_2O_3$ (I) and $Au/La_2O_3$ (II) in CO oxidation (▽), $H_2$ oxidation (○), and POM (□) in the temperature range of 25−300 °C. In POM, the applied $MeOH/O_2$ ratio was 2, and in CO and $H_2$ oxidation a 1:1 molar ratio with oxygen was used. The applied heating rate was 3 °C $min^{-1}$.

clusters resembled both the experimental spectra, as illustrated in Figure 4, and simulated FEFF spectra reported in the literature.[40,43,44] Different bonding modes (atop, bridging, and 3-fold) and smaller gold clusters, e.g., $Au_6$, have been considered but were found to only affect the shape and intensity of the $\Delta\mu$-signatures in a way that was of no consequence for our qualitative interpretation.

The adsorption of CO on a $Au_{43}$ cluster gives rise to the appearance of a positive feature just above the absorption edge caused by a shift of the absorption edge to lower energy and an increase in the whiteline. Since the $L_{III}$ edge XANES probes the empty states in the d-band, an increase in the number of holes results in an increased whiteline. The increase in whiteline intensity has been observed before and was explained by back-bonding of the Au d-electrons into the $2\pi^*$ molecular orbitals of CO causing a depletion of the Au d-band.[43,44] An increased whiteline was also observed in the experimental and theoretical spectra when exposing a Au cluster to $O_2$.[32,43,44,59] This was explained by the activation of oxygen on a Au atom during CO oxidation while partially oxidizing the Au cluster.

All the $\Delta\mu$-XANES signatures obtained from FEFF8 calculations displayed a similar positive feature between 0 and 5 eV over the edge, all suggesting some sort of oxidation of the gold particles. None of the theoretical spectra showed strong similarity with the experimental $\Delta\mu$-XANES signatures obtained on the lanthanum-promoted catalyst materials. However, when inverting the $\Delta\mu$-XANES signature of $Au_{43}O_2$, simulating the reduction of initially present $Au^{\delta+}$ species, a negative feature similar to the experimental spectra appears. On the basis of the experimental results, we cannot completely rule out that oxidation of the $La_2O_3$-promoted Au particles takes place under POM conditions. However, it would only be a minor effect.

**Catalytic Activity.** The catalyst materials exhibiting the best ($Au/La_2O_3$) and worst ($Au/Al_2O_3$) selectivity in POM were compared in the catalytic performance in POM, CO oxidation, and $H_2$ oxidation. The temperature-dependent conversions are presented in Figure 6. It is clear that in terms of MeOH conversion both catalysts behave very comparable. The light-off temperature is found at around 50 °C, and full $O_2$ conversion (plateau between 100 and 200 °C) is reached at 100 °C. At 300 °C, $Au/Al_2O_3$ establishes a somewhat higher conversion, 84% compared to 74% in the case of $Au/La_2O_3$. The strong similarity in MeOH oxidation activity is in line with the similarity in particle size as observed from EXAFS analysis (vide infra) and suggests that the activity is mainly determined by the subnanometer gold particles rather than the larger agglomerates which are observed with TEM. When looking at the results for CO and $H_2$ oxidation, large differences in operation temperature are found. Where the $Au/Al_2O_3$ converts already >40% CO at room temperature, the $Au/La_2O_3$ catalyst is virtually inactive, displaying a conversion of only 5%. The same is observed for $H_2$ oxidation. The $Au/Al_2O_3$ catalyst material is able to oxidize $H_2$ at room temperature; in the case of $Au/La_2O_3$, the light-off temperature for $H_2$ oxidation laid at 100−110 °C, and full $H_2$ conversion was not obtained at 300 °C. Moreover, at temperatures between 100 and 170 °C, the $Au/La_2O_3$ catalyst is more efficient in oxidizing MeOH than $H_2$, opposite to the catalytic performance of $Au/Al_2O_3$. Both catalysts are more efficient in CO oxidation compared to $H_2$ oxidation, which is also reported to be the case for other supported gold nanoparticles.[60]

**Gold Reduction Studied with Differential Scanning Calorimetry.** With DSC one can measure the differences in the heating of a sample compared to a reference, thus revealing endothermic and exothermic events taking place as a function of temperature.[26,61] Since the decomposition of precipitated oxidic gold species is an exothermic process, DSC is a suitable technique to study the reduction behavior of the supported gold-based catalysts.[62] In addition, DSC is performed under $N_2$ atmosphere, in the absence of a reducing agent, similar to the experimental conditions used for catalyst preparation. This is in contrast to TPR, conventionally applied for the study of reduction behavior, which requires the presence of $H_2$. The recorded thermograms of the reduction of the gold-based catalyst are presented in Figure 7 and are compared to the thermograms of the $NH_4OH(aq)$ treated support materials. In the thermograms of the alumina samples, first a negative contribution appeared with a minimum at 120 °C (indicated by "a" in the figure). This can be ascribed to desorption of water from the sample. The decomposition of precipitated oxidic Au-species caused an exothermic peak (indicated by "b" in the figure) in the thermograms between 120 and 170 °C, which is in good agreement with observations reported in the literature.[62] The formation of a metallic Au phase was confirmed by the observed color change after the measurements.

In Table 2, the numerical results for the different samples are listed and compared to the literature values for the direct decomposition of bulk $Au(OH)_3$ according to eq 1[63] and the two-step decomposition via $Au_2O_3$ formation according to eq 2

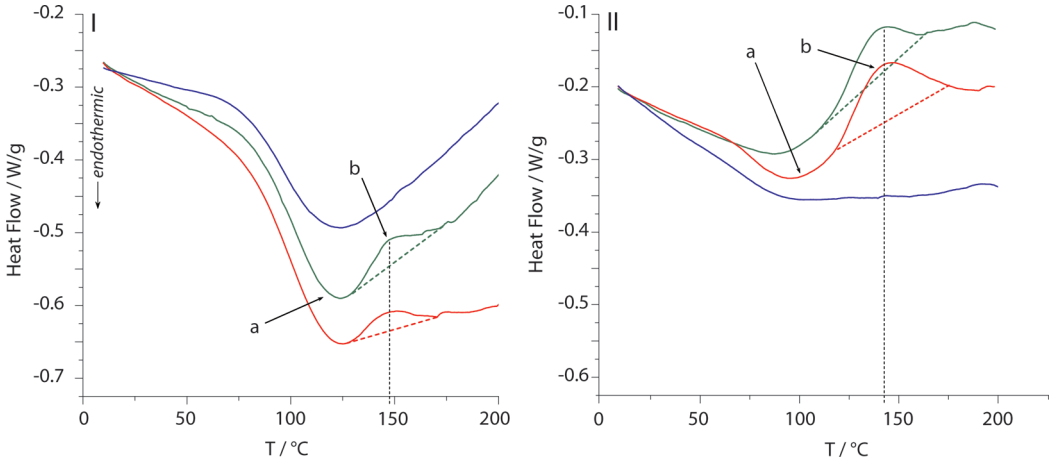


**Figure 7.** Duplicate thermograms of the decomposition of 2.5 wt % precipitated $Au(OH)_x/Au_2O_3$ species (red and green) on $\gamma$-$Al_2O_3$ (I) and $La_2O_3$ (II) studied by DSC and compared with the thermograms of the plain, $NH_4OH$ treated, supports (blue). The applied heating rate was 2 °C $min^{-1}$.

**Table 2. Weight Loading and Numerical Results of the Duplicate Thermal Analysis of the $Au/Al_2O_3$ and $Au/La_2O_3$ Catalyst Materials**

| sample | Au loading[a] (wt %) | weight loss[b] (%) | $T_{max}$[c] (°C) | $-\Delta H_{red}$[c] (J $g^{-1}_{Au}$) |
|---|---|---|---|---|
| $Al_2O_3$ | - | 2.9 | | |
| $Au/Al_2O_3$ | 2.06 | 2.8 | 146 | 81 |
| | | | 147 | 66 |
| $La_2O_3$ | - | 0.74 | | |
| Au/ $La_2O_3$ | 1.23 | 0.68 | 143 | 334 |
| | | | 147 | 352 |
| $Au(OH)_3$ | bulk | | | 20.5[d] |
| $Au_2O_3$ | bulk | | | 50−200[e] |

[a] Determined by ICP analysis. [b] From TG analysis. [c] From DSC measurements. [d] Calculated value for the decomposition of bulk $Au(OH)_3$.[63] [e] Calculated value for the decomposition of $Au_2O_3$.[5,64]

and 3.[5,64]

$$2Au(OH)_3 \rightarrow 2Au + 3H_2O(l) + 1.5O_2(g) \quad \Delta H_f^0 = -20.5\ J\ g_{Au}^{-1} \tag{1}$$

$$2Au(OH)_3 \rightarrow Au_2O_3 + 3H_2O(l) \quad \Delta H_f^0 = +11\ to\ +72\ J\ g_{Au}^{-1} \tag{2}$$

$$Au_2O_3 \rightarrow 2Au + 1.5O_2(g) \quad \Delta H_f^0 = -50\ to\ -200\ J\ g_{Au}^{-1} \tag{3}$$

The measured values for the heat release were significantly higher compared to the heat of reaction for the direct decomposition of $Au(OH)_3$ and therefore cannot be attributed to eq 1. However, the metastable $Au(OH)_3$ can easily dehydrate to form $Au_2O_3$ according to eq 2. Although there is a reasonable spread in the reported values for the heat of formation of $Au_2O_3$, the values we report are roughly in the same order of magnitude as the literature values for the decomposition of $Au_2O_3$ and thus can be considered realistic. Therefore, we propose that by drying the samples under vacuum the precipitated $Au(OH)_3$ species are readily dehydrated to form $Au_2O_3$, which decomposes highly exothermic.

It was found that the measured heat of reaction for the decomposition ($-\Delta H_{red}$) per gram of gold for a $Au/La_2O_3$ catalyst was in all cases roughly 4 times higher than for a $Au/Al_2O_3$ catalyst. Although this is to be regarded as a semiquantitative measurement, the results obtained are reproducible and indicate a significantly higher value for the $-\Delta H_{red}$ for $La_2O_3$ when compared to the $Al_2O_3$-supported samples. Since the formation of gold-aluminate or gold-lanthanate phases is not considered to be realistic under these conditions,[65,66] the difference in measured reduction enthalpy of gold supposedly originates from the extent to which $Au_2O_3$ species are stabilized on the different support materials. Apparently, alumina can stabilize the oxidic gold species to a much higher extent as compared to lanthanum oxide, thus lowering the measured decomposition enthalpy.

## DISCUSSION

In the open literature, there is still a debate on the actual active site for CO oxidation over supported gold particles. Many authors have reported cationic gold atoms, exclusively or together with $Au^0$ atoms, as the active site,[67−74] but also zerovalent metallic gold clusters[44,75−80] and anionic gold species[81−87] have been reported to be needed for CO oxidation. On the basis of density functional theory and ab initio thermodynamic studies, the seemingly contradicting observations were explained by Laursen et al. by the large influence of the support material and reaction conditions on the gold oxidation state.[88] Recently, van Bokhoven et al. reported that $Au/Al_2O_3$ partially forms cationic gold when exposed to oxygen, which gets reduced very fast when introducing CO to the catalyst, proposing a redox cycle of gold during CO oxidation. However, based on the rate-limiting oxygen activation, under CO oxidation reaction, fully reduced gold, with or without CO adsorbed on the surface, is expected.[56,59,89] On the active site of gold catalysts for POM there is very little known. Chang et al. proposed that the active site is a $Au^{\delta+}$ atom, based on ex situ XPS measurements and the observed higher catalytic activity for unreduced gold catalysts on highly reducible supports.[13]

During in situ XAFS experiments under POM conditions, we observed the formation of a positive feature at the edge position in the $\Delta\mu$-XANES spectra of $Au/Al_2O_3$ and $AuBa/Al_2O_3$ showing strong similarity with those reported during hydrogen chemisorption on $Au/Al_2O_3$. Also, the $Au/Al_2O_3$ exhibited high activity in CO and $H_2$ oxidation. For the $AuLa_2O_3/Al_2O_3$ and $Au/La_2O_3$ catalyst materials, a negative feature appeared at the edge position in the $\Delta\mu$-XANES spectra during POM, which can be explained by the decomposition of initially present oxidic gold species. The $Au/La_2O_3$ displayed much lower activity toward CO and $H_2$ formation, which can be explained by the enhanced gold reduction, which limits $Au^{\delta+}$ formation as proposed to be needed for CO oxidation.[32,59] However, the temperature-dependent activity for MeOH conversion was similar for all materials, which indicates that the activity for MeOH activation is not influenced by support interactions. From DSC measurements on the autoreduction behavior of the uncalcined catalyst materials, it was observed that $Au/La_2O_3$ exhibited a significantly larger $-\Delta H_{red}$ than $Au/Al_2O_3$. This is explained by the extent to which $Au_2O_3$ species are stabilized on the different supports. The formation of cationic gold species under POM reaction conditions is consequently facilitated by the alumina support as was observed from in situ XANES.

Although it has been reported before that lanthanum oxide showed remarkable properties for stabilizing cationic gold species,[71,90−92] we observed no indication for the formation of oxidized gold species during POM, as was observed for the $Au/Al_2O_3$ catalyst. On the basis of the combined results of XAS and DSC measurements, FEFF8 simulations, and catalytic performance tests, we propose that the selective catalytic sites for POM are fully reduced gold particles. The presence of $La_2O_3$ clearly limits the oxidation of the gold particles under POM conditions. This inhibits $H_2$ dissociation which was observed on the $Al_2O_3$-supported catalyst and explains the very low methane and water formation when compared to the $Au/Al_2O_3$ catalyst. Consequently a higher selectivity toward $H_2$ formation can be established over a $Au/La_2O_3$ catalyst. Another effect that might play a role is that it is believed that fully reduced gold is the active phase in the water gas shift (WGS) reaction.[93] The enhanced reduction of the $Au/La_2O_3$ catalyst can promote WGS taking place under POM conditions, thus changing selectivities toward more $H_2$ and less CO formation. Although we cannot rule out active participation of the support materials in the mechanism, it is clear that the use of $La_2O_3$ as a support instead of $Al_2O_3$ changes the electronic properties of supported gold catalysts causing different catalytic performance and reduction behavior.

## CONCLUSIONS

With a combination of in situ XAS and DSC measurements, FEFF8 simulations, and catalytic test reactions, we obtained insight into the promotion effect of $La_2O_3$ on supported gold nanoparticles in the partial oxidation of methanol. From the results obtained on the decomposition behavior of precipitated oxidic gold species supported on $La_2O_3$ and $Al_2O_3$, it can be concluded that $La_2O_3$ has a facilitating effect on the decomposition of these oxidic Au species, while $Al_2O_3$ displays a stabilizing effect. This is in agreement with the formation of $Au^{\delta+}$ on the $Au/Al_2O_3$ catalyst during POM, while the $Au/La_2O_3$ catalyst exhibited further decomposition of $Au_2O_3$. It is proposed that the presence of lanthanum oxide facilitates the autoreduction of precipitated oxidic gold species and thereby limits the formation of $Au^{\delta+}$ atoms during partial oxidation of methanol. This prevents dissociative hydrogen chemisorption from taking place, which was observed in the absence of $La_2O_3$. All together, this causes the high selectivity toward $H_2$ in POM. The difference in redox behavior explains the observed activities of the catalyst materials under study in catalytic CO and $H_2$ oxidation, for which the formation of cationic gold species is regarded to be crucial for high activity.

## AUTHOR INFORMATION

### Corresponding Author

*E-mail: b.m.weckhuysen@uu.nl. Phone: +31 (0)30-253 4328. Fax: +31 (0)30-251 1027.

## ACKNOWLEDGMENT

Financial support from ACTS/ASPECT is kindly acknowledged. DUBBLE, NWO−CW, and Hasylab are gratefully thanked for the measurement time. Rob Gosselink, Vincent Koot, Wenhao Luo, and Zoran Ristanovic (all from Utrecht University) and the beamline scientists Sergei Nikitenko (DUBBLE) and Adam Webb (X1) are thanked for their help during the XAFS experiments. The Pharmaceutics Group at Utrecht University is thanked for the use of the DSC and TGA equipment.

## REFERENCES

(1) Bond, G. C.; Sermon, P. A.; Webb, G.; Buchanan, D. A.; Wells, P. B. *J. Chem. Soc., Chem. Commun.* **1973**, *13*, 444b–445.
(2) Haruta, M.; Yamada, N.; Kobayashi, T.; Iijima, S. *J. Catal.* **1989**, *115* (2), 301–309.
(3) Hutchings, G. J. *J. Catal.* **1985**, *96* (1), 292–295.
(4) Della Pina, C.; Falletta, E.; Prati, L.; Rossi, M. *Chem. Soc. Rev.* **2008**, *37* (9), 2077–2095.
(5) Bond, G. C. *Catal. Today* **2002**, *72* (1−2), 5–9.
(6) Bond, G. C.; Thompson, D. T. *Catal. Rev.* **1999**, *41* (3−4), 319–388.
(7) Hutchings, G. J. *Catal. Today* **2005**, *100* (1−2), 55–61.
(8) Haruta, M. *Nature* **2005**, *437* (7062), 1098–1099.
(9) Corma, A.; Leyva-Pérez, A.; Sabater, M. J. *Chem. Rev.* **2011**, *111* (3), 1657–1712.
(10) Chang, F. W.; Lai, S. C.; Roselin, L. S. *J. Mol. Catal. A: Chem.* **2008**, *282* (1−2), 129–135.
(11) Chang, F. W.; Ou, T. C.; Roselin, L. S.; Chen, W. S.; Lai, S. C.; Wu, H. M. *J. Mol. Catal. A: Chem.* **2009**, *313* (1−2), 55–64.
(12) Chang, F. W.; Roselin, L. S.; Ou, T. C. *Appl. Catal. A: Gen.* **2008**, *334* (1−2), 147–155.
(13) Chang, F. W.; Yu, H. Y.; Roselin, L. S.; Yang, H. C.; Ou, T. C. *Appl. Catal. A: Gen.* **2006**, *302* (2), 157–167.
(14) Ou, T. C.; Chang, F. W.; Roselin, L. S. *J. Mol. Catal. A: Chem.* **2008**, *293* (1−2), 8–16.
(15) Yang, H. C.; Chang, F. W.; Roselin, L. S. *J. Mol. Catal. A: Chem.* **2007**, *276* (1−2), 184–190.
(16) Hereijgers, B. P. C.; Weckhuysen, B. M. *ChemSusChem* **2009**, *2* (8), 743–748.
(17) Schlapbach, L.; Züttel, A. *Nature* **2001**, *414*, 353.
(18) Trimm, D. L.; Ilsen Önsan, Z. *Catal. Rev. Sci. Eng.* **2001**, *34* (1−2), 31.
(19) Cheng, W.-H. *Appl. Catal. A: Gen.* **1995**, *130*, 13–30.
(20) Basile, A.; Parmaliana, A.; Tosti, S.; Iulianelli, A.; Gallucci, F.; Espro, C.; Spooren, J. *Catal. Today* **2008**, *137* (1), 17–22.
(21) Perez-Hernandez, R.; Galicia, G. M.; Anaya, D. M.; Palacios, J.; Angeles-Chavez, C.; Arenas-Alatorre, J. *Int. J. Hydrogen Energy* **2008**, *33* (17), 4569–4576.

(22) Turco, M.; Bagnasco, G.; Cammarano, C.; Senese, P.; Costantino, U.; Sisani, M. *Appl. Catal. B: Environ.* **2007**, *77* (1−2), 46–57.
(23) Navarro, R. M.; Pena, M. A.; Fierro, J. L. G. *Chem. Rev.* **2007**, *107* (10), 3952–3991.
(24) Yang, C.; Costamagna, P.; Srinivasan, S.; Benziger, J.; Bocarsly, A. B. *J. Power Sources* **2001**, *103*, 1–9.
(25) Kreuer, K. D. *J. Membr. Sci.* **2001**, *185* (1), 29–39.
(26) Eggenhuisen, T. M.; van Steenbergen, M. J.; Talsma, H.; de Jongh, P. E.; de Jong, K. P. *J. Phys. Chem. C* **2009**, *113* (38), 16785–16791.
(27) Nikitenko, S.; Beale, A. M.; Van Der Eerden, A. M. J.; Jacques, S. D. M.; Leynaud, O.; O'Brien, M. G.; Detollenaere, D.; Kaptein, R.; Weckhuysen, B. M.; Bras, W. *J. Synchrotron Rad.* **2008**, *15* (6), 632–640.
(28) Newville, M. *J. Synchrotron Radiat.* **2001**, *8*, 322–324.
(29) Ravel, B.; Newville, M. *J. Synchrotron Radiat.* **2005**, *12*, 537–541.
(30) Daniel, M. C.; Astruc, D. *Chem. Rev.* **2004**, *104*, 239.
(31) de Graaf, J.; van Dillen, A. J.; de Jong, K. P.; Koningsberger, D. C. *J. Catal.* **2001**, *203* (2), 307–321.
(32) Miller, J. T.; Kropf, A. J.; Zha, Y.; Regalbuto, J. R.; Delannoy, L.; Louis, C.; Bus, E.; van Bokhoven, J. A. *J. Catal.* **2006**, *240* (2), 222–234.
(33) Beale, A. M.; Weckhuysen, B. M. *Phys. Chem. Chem. Phys.* **2010**, *12* (21), 5562–5574.
(34) Sacaliuc, E.; Beale, A. M.; Weckhuysen, B. M.; Nijhuis, T. A. *J. Catal.* **2007**, *248* (2), 235–248.
(35) Teliska, A.; O'Grady, W. E.; Ramaker, D. E. *J. Phys. Chem. B* **2005**, *109* (16), 8076–8084.
(36) Ramaker, D. E.; Koningsberger, D. C. *Phys. Chem. Chem. Phys.* **2010**, *12* (21), 5514–5534.
(37) Ramaker, D. E.; Koningsberger, D. C. *Phys. Rev. Lett.* **2002**, *89* (13), 1.
(38) Nijhuis, T. A.; Sacaliuc, E.; Beale, A. M.; van der Eerden, A. M. J.; Schouten, J. C.; Weckhuysen, B. M. *J. Catal.* **2008**, *258* (1), 256–264.
(39) Arruda, T. M.; Shyman, B.; Ziegelbauer, J. M.; Mukerjee, S.; Ramaker, D. E. *J. Phys. Chem. C* **2008**, *112*, 18087–18097.
(40) Bus, E.; Ramaker, D. E.; van Bokhoven, J. A. *J. Am. Chem. Soc.* **2007**, *129* (26), 8094–8102.
(41) Bus, E.; van Bokhoven, J. A. *Phys. Chem. Chem. Phys.* **2007**, *9* (22), 2894–2902.
(42) Bus, E.; Miller, J. T.; van Bokhoven, J. A. *J. Phys. Chem. B* **2005**, *109* (30), 14581–14587.
(43) Weiher, N.; Beesley, A. M.; Tsapatsaris, N.; Delannoy, L.; Louis, C.; van Bokhoven, J. A.; Schroeder, S. L. M. *J. Am. Chem. Soc.* **2007**, *129*, 2240–2241.
(44) Weiher, N.; Bus, E.; Delannoy, L.; Louis, C.; Ramaker, D. E.; Miller, J. T.; van Bokhoven, J. A. *J. Catal.* **2006**, *240* (2), 100–107.
(45) Koningsberger, D. C.; Oudenhuijzen, M. K.; Bitter, J. H.; Ramaker, D. E. *Top. Catal.* **2000**, *10* (3−4), 167–177.
(46) Ramaker, D. E.; Mojet, B. L.; Oostenbrink, M. T. G.; Miller, J. T.; Koningsberger, D. C. *Phys. Chem. Chem. Phys.* **1999**, *1* (9), 2293–2302.
(47) Ramaker, D. E.; van Dorssen, G. E.; Mojet, B. L.; Koningsberger, D. C. *Top. Catal.* **2000**, *10* (3−4), 157–165.
(48) Vaarkamp, M.; Miller, J. T.; Modica, F. S.; Koningsberger, D. C. *J. Catal.* **1996**, *163* (2), 294–305.
(49) Vaarkamp, M.; Mojet, B. L.; Kappers, M. J.; Miller, J. T.; Koningsberger, D. C. *J. Phys. Chem.* **1995**, *99* (43), 16067–16075.
(50) Ankudinov, A. L.; Rehr, J. J.; Low, J.; Bare, S. R. *Phys. Rev. Lett.* **2001**, *86* (8), 1642–1645.
(51) Oudenhuijzen, M. K.; van Bokhoven, J. A.; Miller, J. T.; Ramaker, D. E.; Koningsberger, D. C. *J. Am. Chem. Soc.* **2005**, *127*, 1530–1540.
(52) Ankudinov, A. L.; Rehr, J. J.; Low, J.; Bare, S. R. *Phys. Rev. Lett.* **2002**, *89* (13), 139702.
(53) Singh, J.; Lamberti, C.; van Bokhoven, J. A. *Chem. Soc. Rev.* **2010**, *39* (12), 4754–4766.
(54) Rupprechter, G. *Catal. Today* **2007**, *126* (1−2), 3–17.
(55) Boccuzzi, F.; Chiorino, A.; Manzoli, M.; Andreeva, D.; Tabakova, T. *J. Catal.* **1999**, *188* (1), 176–185.
(56) Costello, C. K.; Guzman, J.; Yang, J. H.; Wang, Y. M.; Kung, M. C.; Gates, B. C.; Kung, H. H. *J. Phys. Chem. B* **2004**, *108* (33), 12529–12536.
(57) Ankudinov, A. L.; Ravel, B.; Rehr, J. J.; Conradson, S. D. *Phys. Rev. B* **1998**, *58* (12), 7565–7576.
(58) Bus, E.; van Bokhoven, J. A. *J. Phys. Chem. C* **2007**, *111* (27), 9761–9768.
(59) Van Bokhoven, J. A.; Louis, C.; Miller, J. T.; Tromp, M.; Safonova, O. V.; Glatzel, P. *Angew. Chem., Int. Ed.* **2006**, *45* (28), 4651–4654.
(60) Okumura, M.; Nakamura, S.; Tsubota, S.; Nakamura, T.; Azuma, M.; Haruta, M. *Catal. Lett.* **1998**, *51* (1−2), 53–58.
(61) Eggenhuisen, T. M.; den Breejen, J. P.; Verdoes, D.; de Jongh, P. E.; de Jong, K. P. *J. Am. Chem. Soc.* **2010**, *132* (51), 18318–18325.
(62) Viniegra, M.; Asomoza, M.; Gòmez, R. *React. Kinet. Catal. Lett.* **1985**, *28* (2), 389–394.
(63) Roine, A. *HSC Chemistry*, 4th ed.; Outokompu Research Oy: Pori, Finland, 1999.
(64) Buehrer, T. F.; Roseveare, W. E. *J. Am. Chem. Soc.* **1927**, *49*, 1989.
(65) Piao, H.; McIntyre, N. S. *Surf. Sci.* **1999**, *421* (3), L171–L176.
(66) McMasters, O. D.; Gscheidner, K. A.; Bruzzone, G.; Palenzona, A. *J. Less-Common Met.* **1971**, *25*, 135–160.
(67) Hutchings, G. J.; Hall, M. S.; Carley, A. F.; Landon, P.; Solsona, B. E.; Kiely, C. J.; Herzing, A.; Makkee, M.; Moulijn, J. A.; Overweg, A.; Fierro-Gonzalez, J. C.; Guzman, J.; Gates, B. C. *J. Catal.* **2006**, *242* (1), 71–81.
(68) Fierro-Gonzalez, J. C.; Guzman, J.; Gates, B. C. *Top. Catal.* **2007**, *44* (1−2), 103–114.
(69) Guzman, J.; Carrettin, S.; Fierro-Gonzalez, J. C.; Hao, Y. L.; Gates, B. C.; Corma, A. *Angew. Chem., Int. Ed.* **2005**, *44* (30), 4778–4781.
(70) Guzman, J.; Gates, B. C. *J. Am. Chem. Soc.* **2004**, *126* (9), 2672–2673.
(71) Fierro-Gonzalez, J. C.; Bhirud, V. A.; Gates, B. C. *Chem. Commun.* **2005**, 5275–5277.
(72) Guzman, J.; Gates, B. C. *J. Phys. Chem. B* **2002**, *106* (31), 7659–7665.
(73) Guzman, J.; Gates, B. C. *J. Phys. Chem. B* **2003**, *107* (10), 2242–2248.
(74) Fierro-Gonzalez, J. C.; Gates, B. C. *Chem. Soc. Rev.* **2008**, *37* (9), 2127–2134.
(75) Okumura, M.; Tsubota, S.; Haruta, M. *J. Mol. Catal. A: Chem.* **2003**, *199* (1−2), 73–84.
(76) Calla, J. T.; Davis, R. J. *Ind. Eng. Chem. Res.* **2005**, *44* (14), 5403–5410.
(77) Calla, J. T.; Davis, R. J. *J. Phys. Chem. B* **2005**, *109* (6), 2307–2314.
(78) Calla, J. T.; Davis, R. J. *Catal. Lett.* **2005**, *99* (1−2), 21–26.
(79) Wang, H.-F.; Gong, X.-Q.; Guo, Y.-L.; Guo, Y.; Lu, G.; Hu, P. *J. Phys. Chem. C* **2009**, *113* (15), 6124–6131.
(80) Xu, C.; Su, J.; Xu, X.; Liu, P.; Zhao, H.; Tian, F.; Ding, Y. *J. Am. Chem. Soc.* **2007**, *129* (1), 42–43.
(81) Socaciu, L. D.; Hagen, J.; Bernhardt, T. M.; Wöste, L.; Heiz, U.; Häkkinen, H.; Landman, U. *J. Am. Chem. Soc.* **2003**, *125* (34), 10437–10445.
(82) Sanchez, A.; Abbet, S.; Heiz, U.; Schneider, W. D.; Häkkinen, H.; Barnett, R. N.; Landman, U. *J. Phys. Chem. A* **1999**, *103* (48), 9573–9578.
(83) Häkkinen, H.; Abbet, S.; Sanchez, A.; Heiz, U.; Landman, U. *Angew. Chem., Int. Ed.* **2003**, *42* (11), 1297–1300.
(84) Yoon, B.; Häkkinen, H.; Landman, U.; Wörz, A. S.; Antonietti, J. M.; Abbet, S.; Judai, K.; Heiz, U. *Science* **2005**, *307* (5708), 403–407.
(85) Yan, Z.; Chinta, S.; Mohamed, A. A.; Fackler, J. P., Jr; Goodman, D. W. *J. Am. Chem. Soc.* **2005**, *127* (6), 1604–1605.
(86) Molina, T.; Hammer, B. *Phys. Rev. B* **2004**, *69*, 155424.

(87) Minato, T.; Susaki, T.; Shiraki, S.; Kato, H. S.; Kawai, M.; Aika, K. *Surf. Sci.* **2004**, *1012*, 566–568.
(88) Laursen, S.; Linic, S. *Phys. Rev. Lett.* **2006**, *97*, 026101.
(89) Winkler, C.; Carew, A. J.; Haq, S.; Raval, R. *Langmuir* **2003**, *19* (3), 717–721.
(90) Mihaylov, M.; Ivanova, E.; Hao, Y.; Hadjiivanov, K.; Gates, B. C.; Knozinger, H. *Chem. Commun.* **2008**, 175–177.
(91) Goguet, A.; Ace, M.; Saih, Y.; Sa, J.; Kavanagh, J.; Hardacre, C. *Chem. Commun.* **2009**, 4889–4891.
(92) Mihaylov, M.; Ivanova, E.; Hao, Y.; Hadjiivanov, K.; Knozinger, H.; Gates, B. C. *J. Phys. Chem. C* **2008**, *112* (48), 18973–18983.
(93) Burch, R. *Phys. Chem. Chem. Phys.* **2006**, *8*, 5483–5500.